Passivity–Based Control of Power Systems Considering Hydro–Turbine with Surge Tank

Walter Gil-González*, *Member, IEEE*, Alejandro Garces*, *Senior Member, IEEE*,
Olav Bjarte Fosso†, *Senior Member, IEEE*, Andrés Escobar-Mejía*, *Member, IEEE*

***Abstract*—This paper proposes an interconnection and damping assignment passivity-based control (IDA-PBC) for multimachine power systems including hydro-turbine governing systems (HTGS) with surge tank. The main objective is to stabilize the rotor speed and regulate the terminal voltage of each synchronous machine in a power system. The proposed control is decentralized, thus avoiding challenges of communication between generators. Passivity theory is used since the open-loop of the HTGS presents a port-Hamiltonian structure. IDA-PBC allows a control law that maintains the passive structure in closed-loop, guaranteeing its asymptotic stability using Lyapunov's theory. The dynamics of each HTGS are described by an eleventh-order model, which can be reduced to a tenth-order. The proposed control is tested in a 12-bus test system and compared to a standard control, which considers a voltage regulator and exciter based on the IEEE type ST1A excitation system model and power system stabilizer IEEE-PSS1A. The governing system based on a PID control with static and transient droop is also employed. Additionally, the proposed controller is compared to a sliding mode controller. Time-domain simulations demonstrate the robustness and appropriate performance of the proposed decentralized control under different large disturbances.**

***Index Terms*—Passivity-based control, decentralized control, hydro-turbine governing systems, multimachine power system.**

I. Introduction

The components of a power system require to maintain synchronization during and after large disturbances such as fault, loss of a generator, loss of lines or loads, and/or sudden changes in the tie-line flow [1], [2]. The controls of the hydro-generators are responsible for maintaining the terminal voltages and rotor speeds close to the reference value, and injecting sufficient power to damp oscillations and by this, contributing to the overall objective. Therefore, a precise study of the dynamic behavior and stability of hydro-generators is required to guarantee stability [3].

However, there is a trend towards the use of fluctuating loads and generation that can deteriorate the performance of electric power systems. Hydroelectric power plants can play an important role in the frequency regulation and the power balancing [4]–[6] in this new context. In addition, low-frequency oscillation phenomena in hydro-dominated systems have been noted in different countries (see [4] for the Colombian case), which has motivated the study of improved regulation performance for hydro-turbine governing systems (HTGSs) in order to guarantee stable operation of the power system. Nevertheless, HTGS is a complex non-linear system with an intrinsic non-minimum phase characteristic, which has a strong coupling among mechanical, hydraulic and electrical dynamics, making it a difficult system to analyze [6], [7]. Additionally, some other factors such as the appearance and attenuation of the water hammer phenomenon and the large disturbances of the power system hamper the design of a control from a non-linear perspective which simultaneously covers the entire dynamics of the hydraulic, mechanical and electrical parts [6], [8]–[10]. For this reason, the control of HTGS is usually designed from a small signal perspective while separating the dynamics of each subsystem.

Today, most HTGSs are equipped with cascade controllers for the governor subsystem [11], [12] and the automatic voltage regulator (AVR) as well as for the power system stabilizer (PSS) which is usually connected to the excitation system [13], [14]. These controllers can be complicated, having a combination of proportional, integral and derivative properties. The controls are designed and tuned for the worst-case condition and tested by perturbing the closed-loop system under several transient conditions [14]. Even though this technique has been used for many years, it does not guarantee global stability and would not be sufficient in the modern power systems with the integration of distributed resources such as wind power and photovoltaics (PV). Therefore, it is essential to investigate non-linear techniques with high performance that guarantee the power system stability after large disturbances.

Recently, investigations focusing on studying new control schemes for improving the dynamic response of HTGS have been conducted. Some of these investigations consider uncertain parameters or unknown dynamics such as those presented in [15] and [16]. Other investigations have been developed to reduce undesirable oscillations by employing hybrid fuzzy sliding mode controls [17] or sliding mode controls [18]. In [19], a non-linear predictive control method for a HTGS is presented which uses a performance index with a terminal penalty function that guarantees stability in the sense of Lyapunov for discrete systems. In [20], a complementary control strategy was proposed for a governing system to regulate the frequency in an island AC network at sending terminal of the high-voltage direct current system. The authors of [21] established the dynamic model for a pump-turbine considering the non-

This work was partially supported by the National Scholarship Program Doctorates of the Administrative Department of Science, Technology and Innovation of Colombia (COLCIENCIAS).

* Universidad Tecnológica de Pereira. AA: 97-Postcode: 660003-Pereira, Colombia. E-mail: {wjgil,alejandro.garces,andreses1}@utp.edu.co https://orcid.org/0000-0001-7609-1197 - http://orcid.org/0000-0001-6496-05

† Department of Electric Power Engineering, Norwegian University of Science and Technology, 7491 Trondheim, Norway. E-mail: olav.fosso@ntnu.no https://orcid.org/0000-0002-3460-5839

linear piece-wise function of relative parameters. In [22], the impacts of the PI gains in a pumped-storage hydroelectric power plant by introducing the random power load were studied. In [23], a novel approach was proposed to establish the transient modeling of the HTGS. In [24] an adaptive fast-fuzzy fractional order PID control for the pumped-storage hydro unit employing improved gravitational search algorithm was proposed. Control schemes such as intelligent method control [25], fuzzy control [26], [27], fault tolerant control [28], synergetic control [29], and finite-time control [30] have also been proposed. Even though these techniques appear to be effective and robust in their applications, they have limitations such as the need for parameter tuning, adaptation to requirements of large-scale systems, change of control rules, online optimization processes or problems of stability. Additionally, some of these investigations did not consider the entire dynamics of HTGS (i.e., hydraulic, mechanical and electrical dynamics) and they were neither analyzed in a large-scale power system nor under large disturbances.

On the other hand, other authors have developed controls based on the port-Hamiltonian (pH) representation of the subsystems guaranteeing stability for the HTGS in closed-loop [31]–[35]. These authors used an orthogonal decomposition method known as a generalized Hamiltonian theory to design a control with a pH structure in closed-loop [34], [35]. However, the use of this theory needs to have a precise model of the system and leads to loss of physical interpretation of the control law. The authors of [6] showed that it is possible to achieve an open-loop pH structure of HTGS, generating a control law based on passivity theory that exploits its natural structure and, also guarantees its stability in closed-loop. Nevertheless, these controls have some limitations. Firstly, they use a third-order model of a synchronous machine, which only describe mechanical and excitation flux dynamics. Secondly, they do not consider multimachine systems and apply centralized schemes which could be challenging to implement in large-scale power systems where the HTGS are located in wide geographical areas; therefore, communication between them could be difficult. In contrast to these previous works, this paper proposes a decentralized passivity-based control (PBC) of the HTGS for multimachine power systems to stabilize the rotor speed and regulate the terminal voltage of each HTGS in the system. Additionally, the sixth-order model of synchronous machine is considered.

This paper presents a pH modeling and control structure of HTGS with surge tank to keep track and regulate rotor speeds and terminal voltages in a multimachine power system. The proposed control is decentralized and avoids all problems of communication between the HTGSs. Additionally, the proposed control design is based on passivity theory since the open-loop HTGS has a pH structure. The PBC proposes a control law that maintains the passive structure in closed-loop through interconnection and damping assignment (IDA). This guarantees global asymptotic stability using Lyapunov's theory. The complete dynamics of each HTGS are described by an eleventh-order model, which can be reduced to a tenth-order, eliminating the rotor angle dynamic since the stability of the rotor speed is guaranteed. The proposed control is tested and compared with a standard controller, which considers a voltage regulator and exciter based on the IEEE type ST1A excitation system model and power system stabilizer IEEE-PSS1A. A governing system PID control with static and transient droop is also employed. Additionally, the proposed controller is also compared with a sliding mode controller.

The paper is organized as follows: Section II describes the notations used in the paper. Section III briefly demonstrates the IDA-PBC, Section IV presents the dynamic model of the power system, where the HTGS, the synchronous machine as well as the electrical network models along with their representation in a port-Hamiltonian structure are shown. In Section V, the IDA-PBC design for HTGS is shown. In Section VI, the test system used and the results are described. Finally, in Section VII conclusions and recommendations for future work are provided.

II. Notations

The n-by-n identity matrix is denoted by 1_n, an n–by–n null matrix by 0_n and an n–by–m null matrix by $0_{n\times m}$. The diagonal matrix with diagonal elements $d_1, ..., d_n$ is denoted by $\mathrm{diag}(d_1, ..., d_n)$. $x \in \mathbb{R}^n$ is the state vector and $u \in \mathbb{R}^m,\ (m \leq n)$ is the control action. The gradient of a scalar field y with respect to $x = (x_1, ..., x_n)$ is a vector given by $\frac{\partial y}{\partial x} = \left[\frac{\partial y}{\partial x_1} \ ... \ \frac{\partial y}{\partial x_n}\right]^\top$. Therefore, the gradient is assumed as a column vector.

III. A brief of the IDA–PBC

The IDA-BPC method is a control technique proposed in [36], [37], which allows a design of a feedback loop that stabilizes a non-linear system given by:

$$\dot{x} = f(x) + g(x)u + \xi.$$

This can be rewritten as a pH structure as follows:

$$\mathcal{D}\dot{x} = \left(\mathcal{J}(x) - \mathcal{R}(x)\right)\frac{\partial H}{\partial x} + g(x)u + \xi + b(x), \qquad (1)$$

where $\mathcal{J}(x) = -\mathcal{J}(x)^\top \in \mathbb{R}^{n\times n}$ and $\mathcal{R}(x) = \mathcal{R}(x)^\top \succeq 0 \in \mathbb{R}^{n\times n}$ are the interconnection and damping matrices; $\mathcal{D} = \mathcal{D}^\top \succ 0 \in \mathbb{R}^{n\times n}$ is the inertial matrix and $g(x) \in \mathbb{R}^{n\times m}$ is the input matrix while $\xi \in \mathbb{R}^n$ is an external vector. $b(x) \in \mathbb{R}^n$ is a vector of stable and bounded inputs.

The IDA-PBC allows the design of a feedback loop which in a closed-loop system, takes the Hamiltonian form

$$\mathcal{D}\dot{x} = \left(\mathcal{J}_d - \mathcal{R}_d\right)\frac{\partial H_d}{\partial x}, \qquad (2)$$

where $J_d = -J_d^\top$ and $R_d = R_d^\top \succeq 0$ are the new desired interconnection and damping matrices, respectively. The Hamiltonian function H_d is the total stored energy of the system and needs to fulfill

$$x_d = \mathrm{argmin}(H_d), \qquad (3)$$

where x_d is a given point equilibrium.

After assuming a solution of H_d with the matrices J_d and R_d fixed for the system (1), it is found that

$$g(x)^\perp\left(f(x) + \xi\right) = g(x)^\perp\left(\left(\mathcal{J}_d - \mathcal{R}_d\right)\frac{\partial H_d}{\partial x}\right), \qquad (4)$$

where $g(x)^{\perp}$ is a function such that $g(x)^{\perp}g(x) = 0$ and (3) is satisfied. Therefore, the system (2) in closed-loop is achieved with the control law

$$u = \mathcal{G}\left(\left(\mathcal{J}_d - \mathcal{R}_d\right) \frac{\partial H_d}{\partial x} - f(x) - \xi - b(x) \right), \tag{5}$$

where $\mathcal{G} = \left(g(x)^{\top} g(x)\right)^{-1} g(x)^{\top}$.

A. Stability Analysis

A Lyapunov candidate is defined as:

$$W(x) = H_d(x) - H_d(x_d),$$

which fulfills that is always positive since x_d is the minimum of H_d, that is $W(x) > 0$ for all $x \neq x_d$, in addition, $W(x_d) = 0$, and its temporal derivative is

$$\begin{aligned} \dot{W} = \dot{H}_d &= \left[\frac{\partial H_d}{\partial x}\right]^{\top} \mathcal{D}\dot{x} = \left[\frac{\partial H_d}{\partial x}\right]^{\top} \left(\mathcal{J}_d - \mathcal{R}_d\right) \frac{\partial H_d}{\partial x} \\ &= -\left[\frac{\partial H_d}{\partial x}\right]^{\top} \mathcal{R}_d \frac{\partial H_d}{\partial x}. \end{aligned}$$

The dynamic system (1) is Lyapunov stable with the control law (5) if $R_d \succeq 0,\ (\dot{W} \leq 0)$; in addition, if $R_d \succ 0,\ (\dot{W} < 0)$, then the system is asymptotically stable (see for example [38] for more details about Lyapunov theory).

IV. Power System Modeling

This section presents the power system model, which includes the dynamics of hydraulic, electrical, and mechanical subsystems of each HTGS. Additionally, all dynamics will be condensed into a pH model. It is considered that the power system model is a balanced and the rotor power angle δ is known, therefore, the Park transformation can be employed.

A. Hydraulic-Turbine Model

A dynamic model of a hydraulic turbine with penstock and surge tank has been recommended by the working group on prime mover and energy supply models [11], [39]. In this model, incompressible water is assumed. The dynamic model of a hydraulic turbine with penstock is in per-unit values given by:

$$\begin{aligned} T_{W1}\dot{q}_1 &= 1 - h_s - k_{f1}q_1^2, \\ T_j\dot{h}_s &= q_1 - q_2, \\ T_{W2}\dot{q}_2 &= h_s - h - k_{f2}q_2^2, \\ T_y\dot{y} &= u_y - y, \end{aligned} \tag{6}$$

where h and h_s are the head at turbine and the head at surge tank respectively; q_1 and q_2 are the normalized flow rates of tunnel and penstock respectively, and y denotes the servomotor position; k_{f1} and k_{f2} are friction losses on conduit respectively. T_{W1} and T_{W2} are the starting time of water in tunnel and penstock, respectively; T_j is the storage constant of the surge tank and T_y is the time constant of the servomotor [6]. Hydraulic head can be written as.

$$h = \left(\frac{q_2}{y}\right)^2.$$

To ensure a mathematically stable equilibrium point, the next considerations are made: the water flow rate in normal operation and in per-unit is bounded by q_{nl} and 1, i.e., $q_{nl} < q_2 \leq 1$, and the gain position in per-unit value is bounded between $0 < y \leq 1$. The first consideration is given by the flow of water on conduit, which always moves in the same direction. This condition is necessary for the synchronous machine to deliver active power. The second consideration is a feature of servomotor since its position works bounded (see [32] for more details about this considerations).

B. Mechanical Modeling

Generally, a synchronous machine is composed of two parts: rotor and stator. The rotor consists of a shaft where the turbine torque is balanced by the electrical torque developed by the synchronous machine. The equation of the rotor speed is:

$$\begin{aligned} M\dot{\omega} &= \tau_m - \tau_e - d\omega, \\ \dot{\delta} &= \omega - \omega_b \end{aligned} \tag{7}$$

where δ is the rotor power angle, M is the inertia of the rotor shaft, d is the friction constant, and ω_b is the synchronous speed. τ_m and τ_e are mechanical and electrical torque, which can be written as

$$\begin{aligned} \tau_m &= \frac{A_t q_2^2 \left(q_2 - q_{nl}\right)}{y^2 \omega}, \\ \tau_e &= \psi_q i_d - \psi_d i_q, \end{aligned} \tag{8}$$

where q_{nl} denotes its no-load and A_t represents the proportionality constant of the hydro-turbine [1].

C. Synchronous Machine Modeling

The synchronous machine has three identical circuits connected in the stator called *stator windings* (labeled with letters a, b and c). The circuits in the rotor are called *field and damper windings* (labeled with letters f for field winding and, D and Q for damper windings). All the generator windings are magnetically coupled, i.e. that the flux in each winding depends on the currents in all the other windings [1]. This relation between flux linkage and currents is in the dq reference frame given by

$$\psi = Li,$$

with,

$$L = \begin{bmatrix} L_{11} & L_{12} \\ L_{12}^{\top} & L_{22} \end{bmatrix} \quad L_{11} = \begin{bmatrix} L_d & 0 \\ 0 & L_q \end{bmatrix}$$

$$L_{12} = \begin{bmatrix} L_{md} & L_{md} & 0 \\ 0 & 0 & L_{mq} \end{bmatrix} \quad L_{22} = \begin{bmatrix} L_f & L_{md} & 0 \\ L_{md} & L_D & 0 \\ 0 & 0 & L_Q \end{bmatrix},$$

where L_d and L_q represent the stator direct and quadrature inductances, respectively; L_f denotes the field inductance; L_{md} and L_{mq} are the direct and quadrature magnetization inductances, respectively. $\psi = \mathrm{col}(\psi_d, \psi_q, \psi_f, \psi_D, \psi_Q)$, ψ_d and ψ_q represent the stator direct and quadrature axis flux linkages, ψ_f denotes the field flux, ψ_D, and ψ_Q are the rotor

damping windings flux linkages; $i = \text{col}(i_d, i_q, i_f, i_D, i_Q)$, i_d and i_q represent the stator direct and quadrature axis currents, i_f denotes the field current, i_D and i_Q are the rotor damping winding currents.

The terminal voltage of a synchronous machine is given by:

$$\dot{\psi} = -Ri + J_\omega \psi - v, \tag{9}$$

where $v = \text{col}(v_d, v_q, -v_f, 0, 0)$, v_d and v_q denote the stator direct and quadrature axis voltages, v_f represents the field voltage; $R = \text{diag}(r_s, r_s, r_f, r_D, r_Q)$, r_s denotes the stator resistance, r_f represents the field resistance, r_D and r_Q are the rotor damping winding resistances, and

$$J_\omega = \begin{bmatrix} I(\omega) & 0_{2\times 3} \\ 0_{3\times 2} & 0_3 \end{bmatrix} \quad I(\omega) = \begin{bmatrix} 0 & -\omega \\ \omega & 0 \end{bmatrix}.$$

D. Port-Hamiltonian Model

Starting from the energy properties of the HTGS, it is possible to obtain a mathematical representation of the model given by (6) to (9) in a pH structure. The energy function for the i-th HTGS connected to the power system is given by

$$H_i = H_{ti} + H_{mi} + H_{ei}$$

where H_i is the Hamiltonian energy function for the i-th HTGS, which is composed of the sum of the hydro-turbine energy H_{ti}, mechanical energy H_{mi}, and the electrical energy H_{ei}. The hydro-turbine energy is given by

$$H_{ti} = \frac{1}{2} T_{W1i} x_{1i}^2 + \frac{1}{2} T_{ji} x_{2i}^2 + \frac{A_{ti} x_{3i}^2 (x_{3i} - q_{nli})}{x_{4i}}$$

with, $x_{ti} = \text{col}(q_{1i}, h_{si}, q_{2i}, y_i)$ and $\mathcal{D}_{ti} = \text{diag}(T_{W1i}, T_{ji}, T_{W2i}, T_{yi})$.

The kinetic mechanical energy is defined as a quadratic function of the rotor speed

$$H_{mi} = \frac{1}{2} M \omega_i^2,$$

and, the electrical energy is selected as a quadratic function of the rotor fluxes, i.e.,

$$H_{ei} = \frac{1}{2} \psi_i^\top L_i \psi_i.$$

The dynamic systems from (6), (7), and (9) can be rewritten as

$$\mathcal{D}_i \dot{x}_i = (\mathcal{J}_i - \mathcal{R}_i) \frac{\partial H_i}{\partial x_i} + g_i u_i + \xi_i + b_i, \tag{10}$$

with,

$$\begin{aligned}
x_i &= \text{col}(x_{ti}, \omega_i, \psi_i) = \text{col}(x_1, ..., x_{10}), \\
u_i &= \text{col}(u_{yi}, v_{fi}), \\
b_i &= \text{col}(0, -x_{3i}, x_{2i}, 0, 0, 0, 0, 0, 0, 0), \\
\xi_i &= \text{col}(1, 0, 0, 0, 0, -v_{di}, -v_{qi}, 0, 0, 0), \\
\mathcal{D}_i &= \text{diag}(T_{W1i}, T_{ji}, T_{W2i}, T_{yi}, M_i, L_i^{-1}), \\
g_i &= \begin{bmatrix} 0_{3\times 1} & 1 & 0_{6\times 1}; & 0_{7\times 1} & 1 & 0_{2\times 1} \end{bmatrix}^\top, \\
\mathcal{R}_i &= \text{diag}\left(k_{f1i} x_{1i}, 0, r_{3i}, r_{4i}, d_i, R_i\right) + \mathcal{R}_{2i},
\end{aligned}$$

$$\mathcal{R}_{2i} = \begin{bmatrix} 0_3 & 0_{3\times 2} & 0_{3\times 5} \\ 0_{2\times 3} & \begin{bmatrix} 0 & \frac{1}{2x_{5i}} \\ \frac{1}{2x_{5i}} & 0 \end{bmatrix} & 0_{2\times 5} \\ 0_{5\times 3} & 0_{5\times 2} & 0_5 \end{bmatrix},$$

$$\mathcal{J}_i = \begin{bmatrix} \mathcal{J}_{1i} & 0_{2\times 8} \\ 0_{8\times 2} & \mathcal{J}_{2i} \end{bmatrix} \mathcal{J}_{1i} = \begin{bmatrix} 0 & -1 \\ 1 & 0 \end{bmatrix},$$

$$\mathcal{J}_{2i} = \begin{bmatrix} 0_1 & 0_{1\times 4} & 0_{2\times 3} \\ 0_{3\times 2} & \begin{bmatrix} 0 & \frac{1}{2x_{5i}} & 0 & 0 \\ -\frac{1}{2x_{5i}} & 0 & \psi_{qi} & -\psi_{di} \\ 0 & -\psi_{qi} & 0 & 0 \\ 0 & \psi_{di} & 0 & 0 \end{bmatrix} & 0_3 \\ 0_{4\times 1} & 0_3 & 0_3 \end{bmatrix},$$

$$r_{3i} = \frac{x_{3i}^2 \left(k_{f2i} + \frac{1}{x_{4i}^2}\right)}{\frac{\partial H_i}{\partial x_{3i}}}, \quad r_{4i} = \frac{x_{4i}}{\frac{\partial H_i}{\partial x_{4i}}}.$$

It is important to mention that the dynamic model from (10) does not consider the rotor angle dynamic (also known as power angle). Since the rotor angle does not take part in other dynamics of synchronous machine, its behavior does not affect the rest of the dynamics and it is not necessary to develop the controller. By guaranteeing that the rotor angle will be stable, the angle will converge to a constant value, which can be achieved with the IDA-PBC method described in Section III.

E. Electrical Network Model

A power system may include n generators, m transmission lines and k loads. Here, each HTGS is modeled by (10) and each thermal power plant and their governors are modeled by the IEEEG1 steam turbine model [40]. Their mechanical and electrical models are represented in (8) and (9). Loads and transmission lines are represented by the standard phasor representation neglecting their dynamics as these are significantly faster than the mechanical dynamics of each HTGS [1], [41]. In addition, considering the loads as constant impedances, the electrical network model can be reduced by using Kron's reduction, as follows[1]

$$I = Y(\delta_1, ..., \delta_n) V, \; Y(\cdot) \in \mathbb{R}^{2n \times 2n}$$

where Y is the reduced admittance matrix in the terminal nodes of the synchronous machines, $I = [i_{d1}, i_{q1}, ..., i_{dn}, i_{qn}]^\top$ and $V = [v_{d1}, v_{q1}, ..., v_{dn}, v_{qn}]^\top$ are the vectors of the generator currents (i_{d1} and i_{q1}) and terminal voltage (v_{d1} and v_{q1}), respectively.

It is important to mention that phasor representation is used to compute the equilibrium point of system as shown in [2], [42]. Therefore, the analysis made in this paper is in the time domain and, all the dynamics of the grid are considered.

[1]See [1], [2], [42] for more details.

V. HTGS Control

The control objective for the HTGS is to stabilize the rotor speed and regulate the generator terminal voltage to improve power system stability under small and large disturbances. The control design is based on the IDA-PBC presented in Section III and it is developed assuming that the nominal parameters of HTGS are known and all the states are available for measurement.

A. Controller Design

To apply the IDA-PBC method described in Section III, it is necessary to define the desired total stored H_d, the desired interconnection matrix J_d, and the desired damping matrix R_d. The H_d was chosen as the quadratic function:

$$H_{di} = \frac{1}{2}(x_i - x_{di})^\top \mathcal{D}_i (x_i - x_{di}),$$

where x_{di} is desired equilibrium point for each i-HTGS of the power system, also known as the steady-state vector and its the derivative can be calculated as

$$\frac{\partial H_{di}}{\partial x_i} = \begin{bmatrix} x_{1i} - x_{d1i} \\ x_{2i} - x_{d2i} \\ x_{3i} - x_{d3i} \\ x_{4i} - x_{d4i} \\ x_{5i} - x_{d5i} \\ x_{6i} - x_{d6i} \\ x_{7i} - x_{d7i} \\ x_{8i} - x_{d8i} \\ x_{9i} - x_{d9i} \\ x_{10i} - x_{d10i} \end{bmatrix} = \begin{bmatrix} q_{1i} - q_{1di} \\ h_{si} - h_{sdi} \\ q_{2i} - q_{2di} \\ y_i - y_{di} \\ \omega_i - \omega_b \\ i_i - i_{di} \end{bmatrix}.$$

Now, the matrices J_d and R_d are defined as having a relation between the control aims and control variables, as follows:

$$R_d = \text{diag}(r_{1i}, ..., r_{10i}),$$

$$J_d = \begin{bmatrix} 0_2 & 0_{2\times 3} & 0_{2\times 5} \\ 0_{3\times 2} & \begin{bmatrix} 0 & 0 & 0 \\ 0 & 0 & k_{1i} \\ 0 & -k_{1i} & 0 \end{bmatrix} & 0_{3\times 5} \\ 0_{5\times 2} & 0_{5\times 3} & 0_5 \end{bmatrix},$$

where $r_{ji} > 0 \ \forall \ j = 1, ..., 10$ and $k_{1i} \neq 0$.

If (5) is used, the control laws are:

$$\begin{aligned} u_{yi} =& x_{4i} - k_{2i}(x_{5i} - x_{d5i}) - r_{4i}(x_{4i} - x_{d4i}), \\ v_{fi} =& r_{fi} x_{8i} - r_{8i}(x_{8i} - x_{d8i}). \end{aligned} \tag{11}$$

The governing system typically regulates the rotor speed and manages the electrical power generated by synchronous machine by changing gate position. For this reason, the x_{d3} and x_{d5} were chosen to fulfill this aim. By defining an admissible equilibrium point from (6), it is possible to approximate:

$$x_{d3i} \approx \frac{P_{mdi}}{A_{ti}} + q_{nli} + q_{nli}\left(k_{f1i} + k_{f2i}\right)\left(4P_{mdi} + \frac{1}{2}\right)P_{mdi}^2,$$

with $P_{mdi} = P_{di} + ||i_{dqi}||^2 r_{si}$ and P_{di} is the electrical power generated by the i-synchronous machine, and x_{d5i} is:

$$x_{d5i} = \omega_b.$$

The field current controls the voltage magnitude of the generator terminal, which in the dq reference frame is defined as:

$$v_{ti}^2 = v_{di}^2 + v_{qi}^2. \tag{12}$$

Now, using (9) and (12) at an equilibrium point, it is possible to obtain x_{d8i} to control the terminal voltage magnitude, as

$$x_{d8i} = \frac{v_{qi}^d + r_{si} x_{d7i} + L_{di} x_{d5i} x_{d6i}}{L_{mdi} x_{d5i}}. \tag{13}$$

where

$$v_{qi}^d = \sqrt{v_{ti}^2 - v_{di}^2}.$$

To apply the control laws of (11), it is necessary to compute the non-controlled variables that can be found by defining the left annihilator of g_i as

$$g_i^\perp = \begin{bmatrix} 0_{3\times 4} & 1_3 & 0_3 \end{bmatrix}^\top,$$

and using (4), the non-controlled variables are:

$$\begin{aligned} x_{d4i} =& \frac{d_i x_{5i} - \tau_{mi} + \tau_{ei} + k_{1i} x_{4i} - r_{5i}(x_{5i} - x_{d5i})}{k_{1i}}, \\ x_{d6i} =& \frac{-v_{di} + \psi_{qi} x_{d5i} + (r_{6i} + r_{si}) x_{6i}}{r_{6i}}, \\ x_{d7i} =& \frac{-v_{qi} + \psi_{di} x_{d5i} + (r_{7i} + r_{si}) x_{7i}}{r_{7i}}. \end{aligned}$$

VI. Test System, Simulation and Results

The proposed decentralized control based on the IDA–PBC method was assessed on a 12–bus test system (see Fig. 2) to verify its performance and robustness for maintaining the stability of a power system under large disturbance. The test system was proposed in [43] and is composed of synchronous generators, eight transmission lines, six two–winding transformers, six loads, two capacitors for compensation and one reactor. The component data are given in [43]. In this paper, it is considered that the generators #1, #3, and #4 are hydro–turbines, while the generator #2 is a steam turbine. Nevertheless, the excitation control law given in (13) can be employed in a steam turbine without making any changes. For comparison, each generator has been equipped with IEEE–ST1A excitation systems, power system stabilizers IEEE–PSS1A, and turbine governors. The governing systems with static and transient droop to control the hydraulic turbine speed are also considered and its scheme is illustrated in Fig. 1 (see [1]). Parameters of the hydraulic turbine, and the PSS are presented in [6]. The IEEE–ST1A excitation system parameters can be found in [44]. The control design parameters for PID governing system and their limitations are tuned as recommended in [11]. In addition, a comparison against sliding mode controller (SMC) is also shown, which was proposed in [45]

Additionally, a PV penetration level of 10% using three solar power generations with locations as shown in Fig. 2 is considered. It was assumed that each solar power generation, delivers the same active power under similar operating conditions as the synchronous machine listed in Table I.

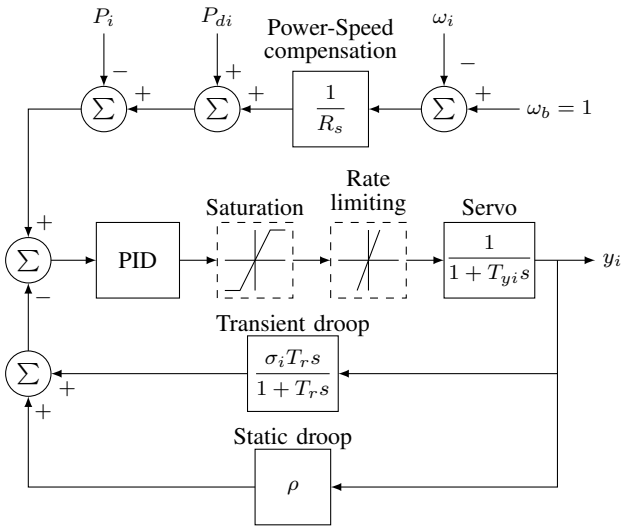

Fig. 1. Block diagram of the governor system with static and transient droop

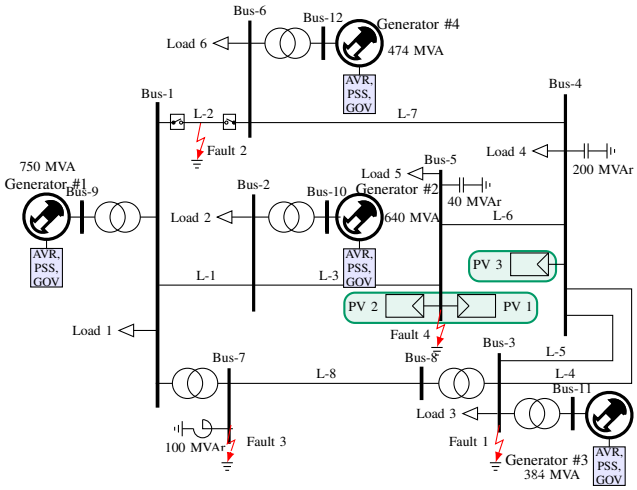

Fig. 2. 12-bus system

TABLE I
OPERATING CONDITION OF EACH SYNCHRONOUS MACHINE

G1		G2		G3		G4	
P	V	P	V	P	V	P	V
3.42	1.00	4.00	1.01	2.70	1.01	3.30	1.01

All data are in per unit. $S_{Base} = 100MW$, $V_{Base} = 230kV$.

Four faults are assumed to demonstrate the robustness and efficiency of the proposed control to improve the dynamic response of the power system with renewable energy integration under large disturbances. The fault #1 is a three-phase to the ground at bus 3 in a period of 200 ms (see Fig. 2). The fault #2 is a short–circuit to the ground permanent at the middle of the transmission line L–2 and the protecting system opens the transmission line after 200 ms. Lastly, the faults #3 and #4 are three-phase to the ground at bus 7 and 5 in a period of 200 ms each them. Here, we considered that the fault #4 occurs to 2.5 s after the fault #3.

To quantify the performance of the control used in this paper, the integral absolute error (IAE) for the rotor speed deviation and the generator terminal voltage is employed, which is computed as follows:

$$\text{IAEW} = \sum_{k=1}^{4} \int_0^{t_{sim}} |\Delta\omega_k| \, tdt,$$

$$\text{IAEV} = \sum_{k=1}^{4} \int_0^{t_{sim}} |\Delta v_{tk}| \, tdt.$$

where t_{sim} is the final simulation time, k denotes each HTGS, $\Delta\omega_k$ is the rotor speed deviation of each generator k, and Δv_{tk} is the difference between the generator terminal voltage k and its voltage reference. The settling time t_s for the rotor speed deviation is also used. Here, the settling time is established when all $|\Delta\omega_k|$ are less than 0.0005 pu, which corresponds to the dead-band for the case of the Colombian power system.

For the sake of simplicity, when referring to standard controls for the HTGS, the interpretation is as follows, the field system is controlled with a IEEE–ST1A excitation system plus a IEEE–PSS1A while the governing system is controlled with the PID control plus a static and a transient droop.

Fault #1

This fault investigates the capacity of the proposed control to maintain the stability and improve the power system dynamic performance with renewable energy integrated during and after a large disturbance.

Fig. 3 shows the dynamic responses of the rotor speed deviation of all synchronous generators. Fig. 3(a) illustrates the rotor speed deviation of generators #1, #2, and #4 when the IDA–PBC is used, while Fig. 3(b) and 3(c) depict the same rotor speed deviations of the generators when SMC and standard controls are employed, respectively. Fig. 3 (d) compares the rotor speed deviation of generator #3 for the controllers. Table II presents the performance indexes for fault #1.

In Fig. 3, it can be noted that the rotor speed deviation of all generators for the proposed controller stabilizes the system in a shorter time and with lower oscillations than other controllers. This is supported by comparing IAEW and t_s between controllers, and these indexes are 51.03% and 50.87% for the proposed controller, respectively.

Fig. 4 illustrates the dynamic responses of the voltage profiles of each synchronous generator. Here, Fig. 4(a) shows the terminal voltages of generators #1, #2, and #4 when the

TABLE II
PERFORMANCE INDEXES

		IAEW	IAEV	t_s [s]
Fault #1	Standard Controllers	49.48	312.56	33.4
	SMC	33.7	224.97	15.37
	IDA-PBC	16.35	133.34	7.55
Fault #2	Standard Controllers	66.34	125.05	5.78
	SMC	32.35	84.57	4.15
	IDA-PBC	2.24	10.17	2.21
Fault #3	Standard Controllers	37.75	676.4	36.4
	SMC	26.55	633.6	15.98
	IDA-PBC	19.75	384.0	6.75

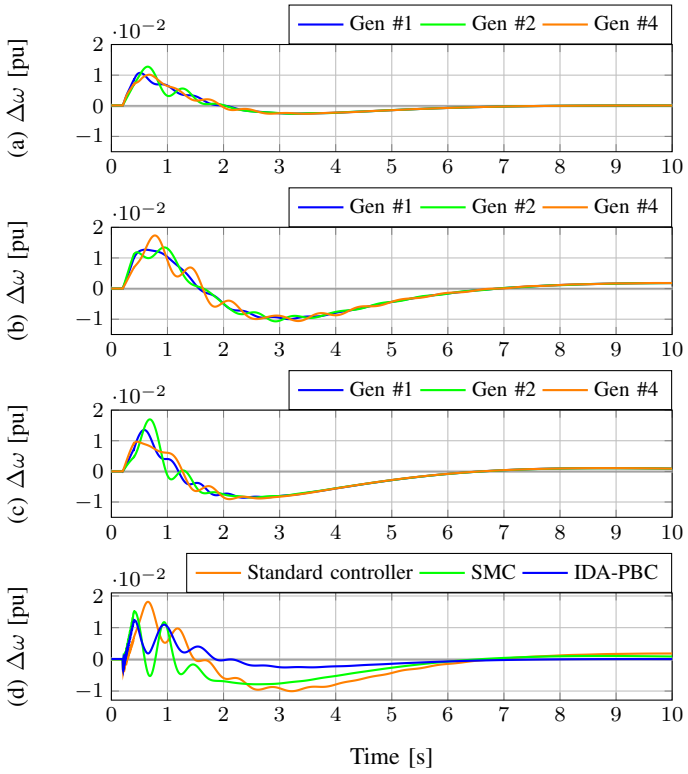

Fig. 3. Dynamic responses of the rotor speed deviation under Fault #1: (a) $\Delta\omega$ using IDA-PBC, (c) $\Delta\omega$ using SMC controller, (c) $\Delta\omega$ using standard controllers, and (d) Control strategy comparison of $\Delta\omega$ in the generator #3.

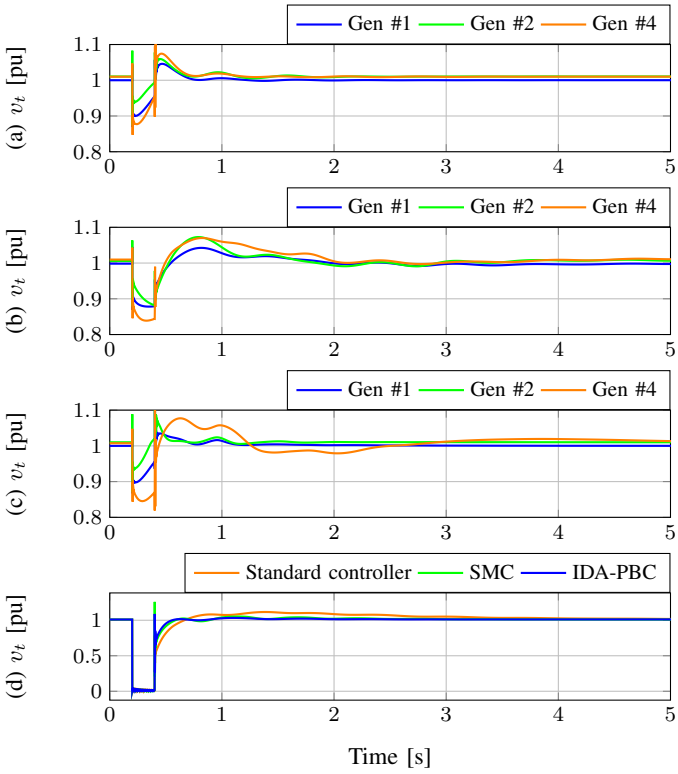

Fig. 4. Dynamic responses of the generator terminal voltages under Fault #1: (a) v_t using IDA-PBC, v_t using SMC controller, (c) v_t using standard controllers, and (c) Control strategy comparison of v_t in the generator #3.

IDA-PBC is implemented, while Fig. 4(b) and 4(c) depict the same generator terminal voltages when the SMC and standard controls are employed, respectively. Fig. 4(d) compares the terminal voltages of generators #3 between controllers.

In Fig. 4, it is observed that the voltage profiles show an improved response when the IDA-PBC is considered. This entails that the proposed control has an enhanced ability to regulate the voltage profiles. This performance is easier to comprehend in Fig. 4(d), where the enhanced response of the proposed control is more clear when the voltage profiles are compared. This can be verified by comparing IAEV between control (see Table II), where this index is lower for the IDA–PBC than the SMC in a 40.73%.

Fault #2

This fault investigates the ability of the IDA-PBC to maintain the stability and improve the dynamic response of a power system when a topology change such as tripping of the transmission line L–2 occurs. Fig. 5 shows the dynamic behavior of the rotor speed deviation of all synchronous generators. Fig. 5(a) depicts the rotor speed deviation of generators #1, #2, and #3 when the IDA-PBC is used, while Fig. 5(b) and 5(c) show the same rotor speed deviation of the generators when the SMC and standard controls are implemented, respectively. Fig. 5(d) compares the rotor speed deviation of generator #4 for between controllers. The performance indexes for fault #2 were shown in Table II.

Fig. 5 shows that the IDA-PBC continues to present an enhanced response of the rotor speed deviation for all generators

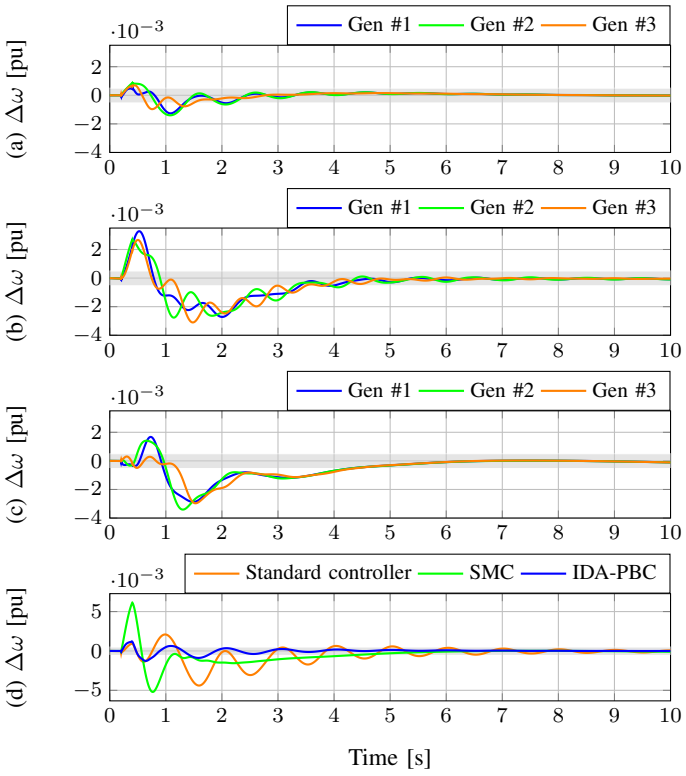

Fig. 5. Dynamic responses of the rotor speed deviation under Fault #2: (a) $\Delta\omega$ using IDA-PBC, (b) $\Delta\omega$ using SMC controller, (c) $\Delta\omega$ using standard controllers, and (c) Control strategy comparison of $\Delta\omega$ in the generator #4.

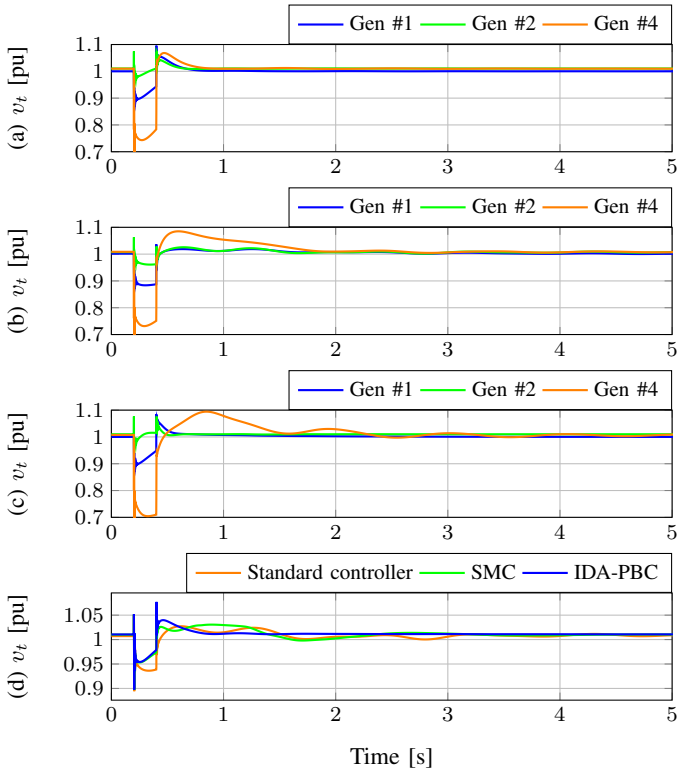

Fig. 6. Dynamic responses of the generator terminal voltages under Fault #2: (a) v_t using IDA-PBC, (b) v_t using SMC controller, (c) v_t using standard controllers, and (c) Control strategy comparison of v_t in the generator #3.

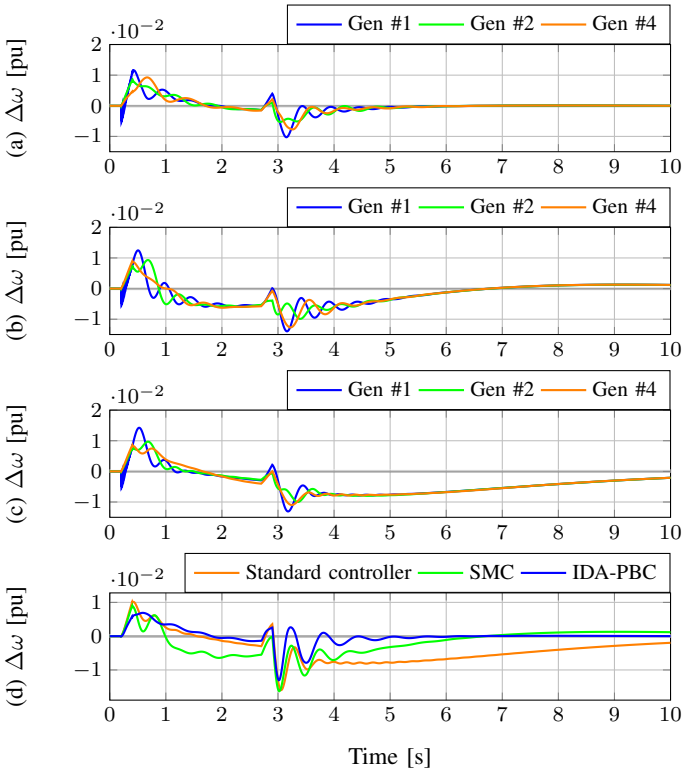

Fig. 7. Dynamic responses of the rotor speed deviation under Fault #3: (a) $\Delta\omega$ using IDA-PBC, (b) $\Delta\omega$ using SMC controller, (c) $\Delta\omega$ using standard controllers, and (c) Control strategy comparison of $\Delta\omega$ in the generator #4.

compared with the SMC and standard controller. Therefore, the power system's dynamic behavior is improved. This can be verified with the performance indexes of Table II, where the IAEW and t_s are lower for the proposed control than the SMC controller with 93.1% and 46.7%, respectively. This difference can be observed clearly in Fig. 5(d) where the frequency oscillations last longer for the SMC and standard controller.

Fig. 6 presents the voltage profile of each synchronous generator for fault #2. Here, Fig. 6(a) shows the terminal voltages of generators #1, #2, and #4 when the IDA-PBC is used, while Fig. 6(b) and 6(c) show the same generator terminal voltages when the SMC and standard controls are implemented, respectively. Fig. 6(d) makes a comparison between the terminal voltages of generator #3.

In Fig. 6, it is observed that the voltage profiles continue to recover faster for the proposed control than the SMC and standard controllers. Here, the IAEV is lower for the IDA-PBC than the SMC and standard control in 87.9% and 91.8%, respectively.

Fault #3

This fault investigates the ability of the IDA-PBC to maintain the stability of a power system when the system has not yet finished recovering from other large disturbance. Fig. 7 depicts the dynamic behavior of the rotor speed deviation of all synchronous generators. Fig. 7(a) shows the rotor speed deviation of generators #1, #2, and #3 when the IDA-PBC is employed, while Fig. 7(b) and 7(c) illustrate the same rotor speed deviation of the generators when the SMC and standard controls are implemented, respectively. Fig. 7(d) compares the rotor speed deviation of generator #3 for between controllers. The performance indexes for fault #3 were shown in Table II.

Note in Fig. 7 that the IDA-PBC continues presenting an improved response of the rotor speed deviation for all generators even when the system has not finished recovering compared with the SMC and standard controller. This entails that the transient response is enhanced. This is supported by the performance indexes of Table II, where the IAEW and t_s are lower for the proposed control than the SMC controller with 25.61% and 57.7%, respectively. The difference between response of the controller can be observed clearly in Fig. 7(d) where the frequency oscillations last longer for the SMC and standard controller.

Fig. 8 presents the voltage profiles of each synchronous generators for fault #3. Here, Fig. 8(a) illustrates the terminal voltages of generators #1, #2, and #4 when the IDA-PBC is implemented, while Fig. 8(b) and 8(c) show the same generator terminal voltages when the SMC and standard controls are used, respectively. Fig. 8(d) shows a comparison between the terminal voltages of generator #3.

Observe in Fig. 8 that the voltage profiles for the proposed control continue to recover faster than the SMC and standard controllers. Note in Table II that the IDA–PBC has the lower IAEV than the SMC and standard controller in 39.3% and 43.1%, respectively.

Complementary analysis

In this part, it is analyzed and computed the efforts of each controller, by using the ITAE = $\int_0^{t_s} \sum_{k=1}^{3} |\Delta u_k|\, dt$, which is

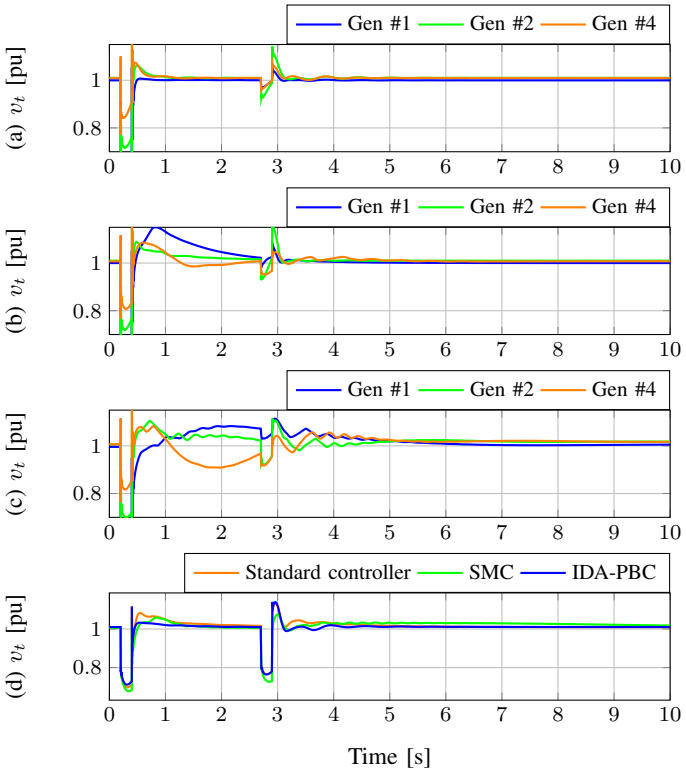

Fig. 8. Dynamic responses of the generator terminal voltages under Fault #3: (a) v_t using IDA-PBC, (b) v_t using SMC controller, (c) v_t using standard controllers, and (c) Control strategy comparison of v_t in the generator #3.

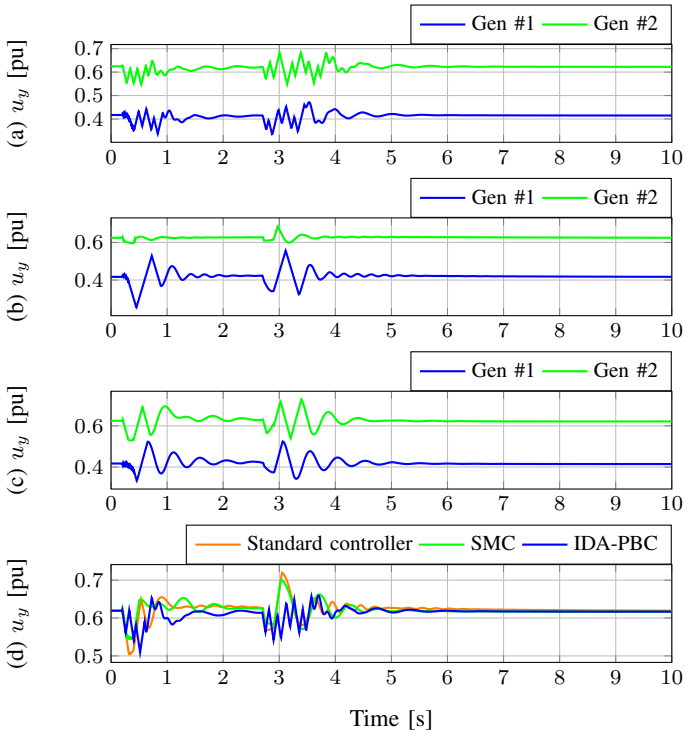

Fig. 9. Control responses for Fault #3: (a) u_y using IDA-PBC, (b) u_y using SMC controller, (c) u_y using standard controllers, and (c) Control strategy comparison of u_y in the generator #1.

presented in Table III. Note that in all the analyzed faults, the IDA–PBC presents lower indexes than the other controllers. This implies that the proposed controller employs less energy and efforts, which is an advantage since it can support higher variations in the power system. Therefore, the IDA-PBC has a broader range of attraction regions compared to the SMC and standard controllers.

Lastly, in Fig. 9 is shown the control inputs u_{yi} to the governor system for fault #3. Here, Fig. 9(a) illustrates the control inputs u_{yi} of the governor systems of generators #1 and #2 when the IDA-PBC is implemented, while Fig. 9(b) and 9(c) depict the same control inputs when the SMC and standard controls are employed, respectively. Fig. 9(d) shows a comparison between the control inputs for the governing system for generator #3.

Observe in Fig. 9(d) that the governor controller law for the IDA–PBC presents greater zigzag than SMC and standard controller since the maximum gate opening rate is used.

TABLE III
PERFORMANCE INDEXES OF EACH CONTROL SCHEME

	u_{yi}		
	Fault #1	Fault #2	Fault #3
Standard Controllers	165.37	53.47	167.22
SMC	105.411	43.54	121.08
IDA–PBC	97.70	37.49	95.46
	v_{fi}		
	Fault #1	Fault #2	Fault #3
Standard Controllers	9825	3474	10323
SMC	8342	4086	12721
IDA–PBC	4861	2491	8615

VII. CONCLUSIONS

An IDA-PBC to control the synchronous machines including HTGS with surge tank in multimachine power systems is proposed. The aims of the proposed control are to stabilize the rotor speed and regulate the terminal voltage of each synchronous machine in the power system. The main advantage of the proposed control is that it is decentralized, thus avoiding the challenges of communication among the generators. Additionally, it keeps the passive structure in closed-loop thus guaranteeing its asymptotic stability based on Lyapunov's theory. The IDA-PBC was assessed on a 12-bus test system and compared with standard controls while considering large disturbances in the power system. It was observed that IDA-PBC had an enhanced transient performance when large disturbances were considered. This is validated with the performance indexes as the settling time, IAEW, and IAEV as these were lower during all fault conditions. This entails that the proposed control improves damping and stability of dynamic systems compared to standard controllers.

As future work, the proposed control will be combined with a methodology for renewable energy sources and energy storage systems to improve transient stability in multimachine power systems.

REFERENCES

[1] J. Machowski, J. W. Bialek, and J. R. Bumby, *Power system dynamics: Stability and Control*, 2nd ed. John Wily & Sons, 2008.

[2] P. Kundur, N. J. Balu, and M. G. Lauby, *Power system stability and control*. McGraw-hill New York, 1994, vol. 7.

[3] W. Yao, L. Jiang, J. Wen, Q. Wu, and S. Cheng, "Wide-area damping controller for power system interarea oscillations: A networked predictive control approach," *IEEE Trans. Control Syst. Techn.*, vol. 23, no. 1, pp. 27–36, 2015.

[4] H. Pico, J. McCalley, A. Angel, R. Leon, and N. Castrillon, "Analysis of very low frequency oscillations in hydro-dominant power systems using multi-unit modeling," *IEEE Trans. Power Syst.*, vol. 27, no. 4, pp. 1906–1915, 2012.

[5] W. Guo, J. Yang, and Y. Teng, "Surge wave characteristics for hydropower station with upstream series double surge tanks in load rejection transient," *Renewable Energy*, vol. 108, pp. 488–501, 2017.

[6] W. Gil-González, A. Garces, and A. Escobar, "Passivity-based control and stability analysis for hydro-turbine governing systems," *Appl. Math. Modell.*, vol. 68, pp. 471–486, 2019.

[7] C. Xu and D. Qian, "Governor design for a hydropower plant with an upstream surge tank by GA-based Fuzzy reduced-order sliding mode," *Energies*, vol. 8, no. 12, pp. 13 442–13 457, 2015.

[8] D. Chen, C. Ding, X. Ma, P. Yuan, and D. Ba, "Nonlinear dynamical analysis of hydro-turbine governing system with a surge tank," *Appl. Math. Modell.*, vol. 37, no. 14, pp. 7611–7623, Aug. 2013.

[9] H. Zhang, D. Chen, C. Wu, and X. Wang, "Dynamics analysis of the fast–slow hydro–turbine governing system with different time–scale coupling," *Commun Nonlinear Sci Numer Simu*, vol. 54, pp. 136–147, 2018.

[10] W. Gil-GonzÁlez, A. Garces, A. Escobar-Mejía, and O. D. Montoya, "Passivity-based control for hydro–turbine governing systems," in *2018 IEEE PES Transmission Distribution Conference and Exhibition - Latin America (T D-LA)*, Sept 2018, pp. 1–5.

[11] IEEE working group report, "Hydraulic turbine and turbine control models for system dynamic studies," *IEEE Trans. Power Syst.*, vol. 7, no. 1, pp. 167–179, Feb 1992.

[12] C. Jiang, Y. Ma, and C. Wang, "PID controller parameters optimization of hydro-turbine governing systems using deterministic-chaotic-mutation evolutionary programming (DCMEP)," *Energy Convers. Manage.*, vol. 47, no. 9, pp. 1222–1230, 2006.

[13] "IEEE recommended practice for excitation system models for power system stability studies - redline," *IEEE Std 421.5-2016 (Revision of IEEE Std 421.5-2005) - Redline*, pp. 1–453, Aug 2016.

[14] H. Huerta, A. Loukianov, and J. Cañedo, "Passivity sliding mode control of large-scale power systems," *IEEE Trans. Control Syst. Technol.*, no. 99, pp. 1–9, 2018.

[15] C. Guan and S. Pan, "Adaptive sliding mode control of electro-hydraulic system with nonlinear unknown parameters," *Control Eng. Pract.*, vol. 16, no. 11, pp. 1275–1284, Nov 2008.

[16] O. Cerman and P. Hušek, "Adaptive fuzzy sliding mode control for electro-hydraulic servo mechanism," *Expert Syst. Appl.*, vol. 39, no. 11, pp. 10 269–10 277, Sep 2012.

[17] J. Liang, X. Yuan, Y. Yuan, Z. Chen, and Y. Li, "Nonlinear dynamic analysis and robust controller design for francis hydraulic turbine regulating system with a straight-tube surge tank," *Mech. Syst. Sig. Process.*, vol. 85, no. Supplement C, pp. 927–946, Feb 2017.

[18] D. Chen, C. Ding, Y. Do, X. Ma, H. Zhao, and Y. Wang, "Nonlinear dynamic analysis for a francis hydro-turbine governing system and its control," *J. Franklin Inst.*, vol. 351, no. 9, pp. 4596–4618, Sep 2014.

[19] R. Zhang, D. Chen, and X. Ma, "Nonlinear predictive control of a hydropower system model," *Entropy*, vol. 17, no. 9, pp. 6129–6149, 2015.

[20] G. Zhang, Y. Cheng, N. Lu, and Q. Guo, "Research of Hydro-turbine Governor Supplementary Control Strategy for Islanding AC Grid at Sending Terminal of HVDC System," *IEEE Trans. Energy Convers.*, vol. 31, no. 4, pp. 1229–1238, 2016.

[21] H. Zhang, D. Chen, C. Wu, X. Wang, J. Lee, and K. Jung, "Dynamic modeling and dynamical analysis of pump-turbines in s-shaped regions during runaway operation," *Energ Conver. Manag.*, vol. 138, pp. 375–382, 2017.

[22] H. Zhang, D. Chen, B. Xu, E. Patelli, and S. Tolo, "Dynamic analysis of a pumped-storage hydropower plant with random power load," *Mechanical Systems and Signal Processing*, vol. 100, pp. 524–533, 2018.

[23] H. Zhang, D. Chen, P. Guo, X. Luo, and A. George, "A novel surface-cluster approach towards transient modeling of hydro-turbine governing systems in the start-up process," *Energy Convers. Manage.*, vol. 165, pp. 861–868, 2018.

[24] Y. Xu, J. Zhou, X. Xue, W. Fu, W. Zhu, and C. Li, "An adaptively fast fuzzy fractional order pid control for pumped storage hydro unit using improved gravitational search algorithm," *Energy Convers. Manage.*, vol. 111, pp. 67–78, 2016.

[25] N. Kishor and S. Singh, "Simulated response of NN based identification and predictive control of hydro plant," *Expert Syst. Appl.*, vol. 32, no. 1, pp. 233–244, 2007.

[26] K. Nagode and I. Škrjanc, "Modelling and internal fuzzy model power control of a francis water turbine," *Energies*, vol. 7, no. 2, pp. 874–889, 2014.

[27] C. Li, Y. Mao, J. Zhou, N. Zhang, and X. An, "Design of a fuzzy-PID controller for a nonlinear hydraulic turbine governing system by using a novel gravitational search algorithm based on Cauchy mutation and mass weighting," *Applied Soft Computing*, vol. 52, pp. 290–305, 2017.

[28] S. Simani, S. Alvisi, and M. Venturini, "Fault tolerant control of a simulated hydroelectric system," *Control Eng. Pract.*, vol. 51, pp. 13–25, 2016.

[29] W. Zhu, Y. Zheng, J. Dai, and J. Zhou, "Design of integrated synergetic controller for the excitation and governing system of hydraulic generator unit," *Eng. Appl. Artif. Intell.*, vol. 58, pp. 79–87, 2017.

[30] C. Ma, C. Liu, X. Zhang, Y. Sun, W. Wu, and J. Xie, "Fixed-time stability of the hydraulic turbine governing system," *Math Probl Eng*, vol. 2018, 2018.

[31] Y. Zeng, L. Zhang, T. Xu, and H. Dong, "Improvement rotor angle oscillation of hydro turbine generating sets based on hamiltonian damping injecting method," in *Power and Energy Engineering Conference (APPEEC), 2010*, May 2010, pp. 1–5.

[32] T. Xu, L. Zhang, Y. Zeng, and J. Qian, "Hamiltonian model of hydro turbine with sharing sommon conduit," in *2012 Asia-Pacific Power and Energy Engineering Conference*, March 2012, pp. 1–5.

[33] Y. Zeng, L. Zhang, Y. Guo, J. Qian, and C. Zhang, "The generalized hamiltonian model for the shafting transient analysis of the hydro turbine generating sets," *Nonlinear Dyn.*, vol. 76, no. 4, pp. 1921–1933, Jun 2014.

[34] B. Xu, F. Wang, D. Chen, and H. Zhang, "Hamiltonian modeling of multi-hydro-turbine governing systems with sharing common penstock and dynamic analyses under shock load," *Energy Convers. Manage.*, vol. 108, pp. 478–487, 2016.

[35] H. Li, D. Chen, H. Zhang, C. Wu, and X. Wang, "Hamiltonian analysis of a hydro-energy generation system in the transient of sudden load increasing," *Appl. Energy*, vol. 185, Part 1, pp. 244–253, 2017.

[36] R. Ortega, A. J. Van Der Schaft, I. Mareels, and B. Maschke, "Putting energy back in control," *IEEE Control Syst. Mag.*, vol. 21, no. 2, pp. 18–33, 2001.

[37] R. Ortega, A. Van Der Schaft, B. Maschke, and G. Escobar, "Interconnection and damping assignment passivity-based control of port-controlled hamiltonian systems," *Automatica*, vol. 38, no. 4, pp. 585–596, 2002.

[38] L. Perko, *Differential equations and dynamical systems*. Springer Science & Business Media, 2013, vol. 7.

[39] J. Jiang, "Design of an optimal robust governor for hydraulic turbine generating units," *IEEE Trans. Energy Convers.*, vol. 10, no. 1, pp. 188–194, Mar 1995.

[40] P. Pourbeik *et al.*, "Dynamic models for turbine-governors in power system studies," *IEEE Task Force on Turbine-Governor Modeling*, no. 2013, 2013.

[41] A. G. Loukianov, H. Huerta, V. Utkin, and J. M. Cañedo, "Nonlinear passivity robust decentralized controller for large scale power system," *IFAC Proceed. Volumes*, vol. 42, no. 4, pp. 474–479, 2009.

[42] P. M. Anderson and A. A. Fouad, *Power system control and stability*. John Wiley & Sons, 2008.

[43] A. Adamczyk, M. Altin, Ö. Göksu, R. Teodorescu, and F. Iov, "Generic 12-bus test system for wind power integration studies," in *Power Electronics and Applications (EPE), 2013 15th European Conference on*. IEEE, 2013, pp. 1–6.

[44] K. Máslo, A. Kasembe, and M. Kolcun, "Simplification and unification of IEEE standard models for excitation systems," *Electr. Power Syst. Res.*, vol. 140, pp. 132–138, 2016.

[45] J. Liang, X. Yuan, Y. Yuan, Z. Chen, and Y. Li, "Nonlinear dynamic analysis and robust controller design for francis hydraulic turbine regulating system with a straight-tube surge tank," *Mechanical Systems and Signal Processing*, vol. 85, pp. 927–946, 2017.